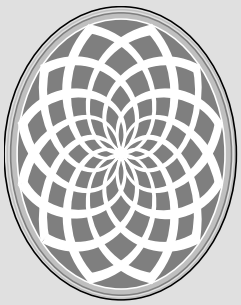

INTERDISCIPLINARY MATHEMATICS INSTITUTE

2011:05

Mass-Conserved Phase Field Models for Binary Fluids

Jie Shen, Xiaofeng Yang and Qi Wang

IMI

PREPRINT SERIES

COLLEGE OF ARTS AND SCIENCES

UNIVERSITY OF SOUTH CAROLINA

Mass-Conserved Phase Field Models for Binary Fluids

Jie Shen[*], **Xiaofeng Yang**[†] and **Qi Wang**[‡]

Abstract

The commonly used incompressible phase field models for non-reactive, binary fluids, in which the Cahn-Hilliard equation is used for the transport of phase variables, conserve the total volume of each phase as well as the material volume, but do not conserve the mass of the fluid mixture when the densities of two components are different. In this paper, we formulate the phase field theory for mixtures of two incompressible fluids, consistent with the quasi-compressible theory [28], to ensure the conservation of mass and momentum for the fluid mixture as well as the volume for each fluid phase. In this formulation, the mass-average velocity is no longer divergence-free (solenoidal) when the densities of two components in the mixture are not equal, making it a compressible model subject to an internal constraint. An efficient numerical method is then devised to enforce this compressible internal constraint. Numerical simulations in confined geometries for both the compressible and the incompressible models are carried out using spatially high order spectral methods to contrast the model predictions. Numerical comparisons show that (a) the predictions by the two models agree qualitatively in the situation where the interfacial mixing layer is thin; and (b) the predictions differ significantly in binary fluid mixtures undergoing mixing with a large mixing zone. The numerical study delineates the limitation of the commonly used incompressible phase field model and thereby cautions its predictive value in simulating well-mixed binary fluids.

1 Introduction

Phase field models have been used successfully to study a variety of interfacial phenomena like equilibrium shapes of vesicle membranes [12, 13, 14, 15, 16, 35], blends of polymeric liquids [36, 37, 38, 17], multiphase fluid flows [19, 23, 24, 28, 25, 41, 40, 42, 43, 44, 45], dentritic growth in solidification, microstructure evolution [21, 29, 22], grain growth [8], crack propagation [9], morphological pattern formation in thin films and on surfaces [26, 30], self-assembly dynamics of two-phase monolayer on an elastic substrate [27], a wide variety of diffusive and diffusion-less solid-state phase transitions [10, 39], dislocation modeling in microstructure, electro-migration and multiscale modeling [34]. Multiple phase-field methods can be devised to study multiphase materials [40]. Recently, phase field models are applied to study liquid crystal drop deformation in another fluid, liquid films, polymer nanocomposites, and biofilms [19, 23, 24, 28, 25, 41, 40, 42, 43, 44, 18, 46, 5].

Comparing to other mathematical and computational technologies available for studying multi-phase materials, the phase-field approach exhibits a clear advantage in its simplicity in model formulation, ease of numerical implementation, and the ability to explore essential interfacial physics at the interfacial regions etc. Computing the interface without explicitly tracking the interface is the most attractive numerical feature

[*]shen@math.purdue.edu, Department of Mathematics, Purdue University, West Lafayette, IN 46907, USA

[†]xfyang@math.sc.edu, Department of Mathematics and NanoCenter at USC, University of South Carolina, Columbia, SC 29028, USA

[‡]qwang@math.sc.edu, Department of Mathematics and NanoCenter at USC, University of South Carolina, Columbia, SC 29028, USA; School of Mathematics, Nankai University, Tianjin, P. R. China, 300071; Beijing Computational Science Research Center, Beijing, P. R. China, 100084

of this modeling and computational technology. Since the pioneering work of Cahn and Hilliard in the 50's of the last century, the Cahn-Hilliard equation has been the foundation for various phase field models [6, 7]. It arises naturally as a model for multiphase fluid mixtures should the entropic and mixing energy of the mixture system be known. For immiscible binary fluid mixtures, one commonly uses a labeling or a phase variable (also known as a volume fraction or an order parameter) ϕ to distinguish between distinct fluid phases. For instance $\phi = 1$ indicates one fluid phase while $\phi = 0$ denotes the other fluid phase in an immiscible binary mixture. The interfacial region is tracked by $0 < \phi < 1$. Given the historical reason, most mixing energies are calculated in terms of the volume fraction instead of the mass fraction in the literature [20, 11]. Consequently, the system free energy including the entropic and mixing contribution has been formulated in the volume fraction as well [20, 11]. We denote the system free energy for the material system to be modeled by $F(\phi, \nabla\phi, \cdots)$. A transport equation for the volume fraction ϕ along with the conservation equation of momentum and continuity equation constitutes the essential part of the governing system of equations for the binary fluid mixture. The volume fraction serves as an interval variable for the fluid mixture.

In the literature on immiscible binary mixtures of incompressible fluids, one uses the concept of chemical potential to formulate the transport equation for the volume fractions of the fluids ϕ_1 and ϕ_2. In this formulation, the material incompressibility is on the one hand modeled by the continuity equation

$$\nabla \cdot \mathbf{v} = 0, \tag{1.1}$$

while on the other hand, interpreted as the invariant property of the sum of the volume fractions for the two fluid components, i.e., $\phi_1 + \phi_2 = 1$ if we denote $\phi = \phi_1$ and $\phi_2 = 1 - \phi$. This assumption is plausible and indeed consistent with the fluid compressibility (1.1) only if the two components are either completely separated by phase boundaries when their densities are not equal or possibly mixed when the densities are identical. Otherwise, there is a potential inconsistency with the usual conservation of mass. This inconsistency has been identified in [28], but ignored by many practitioners using phase field modeling technologies. We note that this inconsistency occurs only in the mixed region of the two incompressible fluids, where the incompressible condition (1.1) is no longer valid, indicating the mixture is no longer incompressible despite that each fluid component participating in mixing is incompressible. This type of fluids is referred to as quasi-compressible in [28].

This paper aims at discussing the inconsistency for binary mixtures of two incompressible fluids of unmatched densities and viscosities and providing a quantitative assessment for the quasi-compressible phase field model that obeys the conservation of both mass and volume against the incompressible one that only respects the volume conservation. The paper is organized as follows. First we discuss the mathematical formulation of the phase field theory for binary viscous fluid mixtures and its various approximations and their ramifications. Secondly, we develop a new set of numerical algorithms, which enforce the mass conservation, to solve the governing system of fluid flow equations. Thirdly, we implement the algorithms using spatially high order spectral methods and discuss the discrepancies between the ad hoc incompressible phase field model and the quasi-compressible phase field model in two representative examples.

2 The mathematical model

We revisit the derivation of the governing system of equations for a binary mixture of incompressible viscous fluids, which includes the transport equation for a phase variable (the volume fraction) and the conservation equations for mass and linear momentum. The conservation equations for a binary system can be formulated in two different ways: either as a two fluid model or a one fluid two component model [1, 4, 2]. For nontrivial fluid simulations, the one fluid multi-component formulation often yields a convenient governing system of equations and easy-to-implement boundary conditions for the model's hydro-dynamical

variables. The phase field theory falls naturally into the one fluid two component formulation [6]. In the phase field formulation, chemical reaction between the two distinct components can take place so that one component can be turned into the other component. However, the overall mass must be conserved. In this paper, we will not address the phase field formulation with chemical reactions. This topic deserves a separate discussion of its own.

2.1 Governing equations

In a phase field theory, the transport equation for the volume fraction of one fluid phase is given by

$$\phi_t + \nabla \cdot (\phi \mathbf{v}) = \nabla \cdot (\lambda \nabla \mu), \tag{2.1}$$

where $\mathbf{v}$ is an average velocity to be clarified below, $\lambda = \lambda(\phi)$ is the mobility function, and $\mu = \frac{\delta F}{\delta \phi}$ is the chemical potential of the material system. The mobility function λ is often taken as a constant λ_0, but is preferably a function of ϕ in the form:

$$\lambda = \lambda_0 \phi (1 - \phi). \tag{2.2}$$

The Cahn-Hilliard equation with the volume fraction dependent mobility is called singular or modified Cahn-Hilliard equation. Often, it is approximated simply by a constant value $\lambda = \lambda_0$ in studying phase separated, immiscible fluids. The resultant equation is the well-known Cahn-Hilliard equation.

The free energy of the mixture system is normally a function of the labeling function of phase function and its higher order derivatives (only the first order is included here for brevity):

$$F = F(\phi, \nabla \phi). \tag{2.3}$$

In this paper, we consider the mixture of two incompressible fluids with constant mass density ρ_1 and ρ_2, respectively. The total density of the mixture is then given by

$$\rho = \rho_1 \phi + \rho_2 (1 - \phi). \tag{2.4}$$

We identify $\mathbf{v}$ as the mass-average velocity for the mixture. Then, the conservation equations for mass and momentum are given by

$$\begin{aligned} &\rho_t + \nabla \cdot (\rho \mathbf{v}) = 0, \\ &(\rho \mathbf{v})_t + \nabla \cdot (\rho \mathbf{v} \mathbf{v}) = \nabla \cdot (\tau) - \phi \nabla \mu + \mathbf{F}_e, \end{aligned} \tag{2.5}$$

where $\mathbf{F}_e$ is the external force and $\phi \nabla \mu$ is the "elastic force" or the "surface force" due to the interfacial energy $f(\phi)$. The surface force $-\phi \nabla \mu$ can be replaced by $\mu \nabla \phi$ modulo a surface term which is normally zero. In light of the transport equation for the volume fraction, we have

$$\rho \nabla \cdot \mathbf{v} = -(\rho_1 - \rho_2)(\phi_t + \mathbf{v} \cdot \nabla \phi) = -(\rho_1 - \rho_2)(\nabla \cdot (\lambda \nabla \mu) - \phi \nabla \cdot \mathbf{v}), \tag{2.6}$$

we then derive from the above and (2.1) that

$$\nabla \cdot \mathbf{v} = \frac{\rho_2 - \rho_1}{\rho_2} [\phi_t + \nabla \cdot (\phi \mathbf{v})] = \frac{\rho_2 - \rho_1}{\rho_2} [\nabla \cdot (\lambda \nabla \mu)]. \tag{2.7}$$

It is apparent that the divergence free condition for the mass-average velocity field is satisfied only if $\rho_1 = \rho_2$ or $\nabla \cdot (\lambda \nabla \mu) = 0$. Otherwise, the mass conservation equation serves as a constraint for the velocity field, which determines the undetermined pressure in the constraint hydrodynamic theory for fluid mixtures. We

note that $\nabla\cdot(\lambda\nabla\mu)$ is normally not zero for a spatially inhomogeneous system. Hence, as long as $\rho_1\neq\rho_2$, eq. (2.7) serves as a constraint.

To close the system of equations, we must come up with a constitutive equation for the stress tensor τ. We consider the mixture made up of viscous fluids. For viscous fluids, the stress constitutive equation is

$$\tau=\tau_c+2\eta\mathbf{D}+\nu tr(\mathbf{D})\mathbf{I}, \tag{2.8}$$

where τ_c is the constraint stress responsible to maintain the constraint eq. (2.7) without any contribution to the entropy production, η is the shear viscosity, ν is the volumetric viscosity, and $\mathbf{D}$ is the rate of strain tensor. The ratio between ν and η depends on the property of the material and is roughly 4.3 for water for example. The viscosity coefficients for the fluid mixture are interpolated through the volume fraction and given by

$$\eta=\eta_1\phi+\eta_2(1-\phi),\nu=\nu_1\phi+\nu_2(1-\phi), \tag{2.9}$$

where $\eta_{1,2},\nu_{1,2}$ are constant shear and volumetric viscosities for fluid 1 and fluid 2, respectively.

To deal with constraint (2.7), we augment the free energy with a term $\bar{F}$ called the constraint response:

$$\mathcal{F}=F+\bar{F}. \tag{2.10}$$

Based on the second law of thermodynamics in the form of the Clausius-Duhem inequality, the constraint response does not contribute to entropy production, i.e.,

$$\tau_c:\mathbf{D}-\frac{\delta\bar{F}}{\delta\phi}\dot{\phi}=0, \tag{2.11}$$

where $\dot{\phi}=\frac{\partial\phi}{\partial t}+\nabla\cdot(\mathbf{v}\phi)$ is the material derivative. We rewrite eq. (2.7) as

$$\mathbf{I}:\mathbf{D}+\frac{\rho_1-\rho_2}{\rho_2}\dot{\phi}=0. \tag{2.12}$$

For eq. (2.11) must be valid for all thermodynamic processes that obeys (2.12), we deduce that

$$\tau_c=-p\mathbf{I} \tag{2.13}$$

where p is the hydrodynamic pressure, and the free energy component ($\bar{F}$) corresponding to the constraint response:

$$\bar{F}=\frac{\rho_1-\rho_2}{\rho_2}\phi p. \tag{2.14}$$

If we choose $\mu=\frac{\delta\mathcal{F}}{\delta\phi}$, we obtain a set of equations that respect the conservation of mass and total volume:

$$\phi_t+\nabla\cdot(\phi\mathbf{v})=\nabla\cdot(\lambda\nabla\mu), \tag{2.15a}$$

$$\begin{aligned}(\rho\mathbf{v})_t+\nabla\cdot(\rho\mathbf{v}\mathbf{v})=\rho[\mathbf{v}_t+\mathbf{v}\cdot\nabla\mathbf{v}]&=\nabla\cdot(2\eta\mathbf{D}+\nu tr(\mathbf{D})\mathbf{I})-\nabla p-\phi\nabla\mu+\mathbf{F}_e\\&=\nabla\cdot(\eta\nabla\mathbf{v})+\nabla((\eta+\nu)\nabla\cdot\mathbf{v})-\nabla p-\phi\nabla\mu+\mathbf{F}_e,\end{aligned} \tag{2.15b}$$

$$\nabla\cdot\mathbf{v}=\frac{\rho_2-\rho_1}{\rho_2}[\nabla\cdot(\lambda\nabla\mu)], \tag{2.15c}$$

$$\mu=\frac{\delta\mathcal{F}}{\delta\phi}=\frac{\delta F}{\delta\phi}+\frac{\rho_1-\rho_2}{\rho_2}p. \tag{2.15d}$$

We refer (2.15) as the compressible model 2 in this paper. On the other hand, if we set $\mu = \frac{\delta F}{\delta \phi}$ in the system of equations listed above, we obtain another set of equations, which we refer as the compressible model 1. With the help of (2.15c), the transport equation for ϕ can be recast into

$$\phi_t + \nabla \cdot (\phi \mathbf{v}) = \frac{\rho_2}{\rho_2 - \rho_1} \nabla \cdot \mathbf{v} \tag{2.16}$$

provided $\rho_1 \neq \rho_2$.

The above compressible models preserve the mass conservation and are compressible inside the mixing/interfacial region. On the other hand, the incompressible model, in which the mass average velocity field is assumed solenoidal, consists of the following equations:

$$\phi_t + \nabla \cdot (\phi \mathbf{v}) = \nabla \cdot (\lambda \nabla \mu), \tag{2.17a}$$

$$\rho[\mathbf{v}_t + \mathbf{v} \cdot \nabla \mathbf{v}] = \nabla \cdot (\eta \nabla \mathbf{v})) - \nabla p - \phi \nabla \mu + \mathbf{F}_e, \tag{2.17b}$$

$$\nabla \cdot \mathbf{v} = 0, \tag{2.17c}$$

$$\mu = \frac{\delta F}{\delta \phi}. \tag{2.17d}$$

This model assumes that the flow is incompressible everywhere at the expense of local mass conservation inside the interfacial/mixing region.

For the compressible models, we define the total energy as

$$\mathcal{E}(t) = \int_\Omega [\frac{\rho \|\mathbf{v}\|^2}{2} + \mathcal{F}] d\mathbf{x}, \tag{2.18}$$

where $\mathbf{x}$ is the Eulerian coordinate. For compressible model 1, the rate of change in the total energy is given by

$$\frac{d\mathcal{E}}{dt} = -\int_\Omega [\lambda \|\nabla \mu\|^2 + (\tau - \tau_c) : \mathbf{D}] d\mathbf{x} + \frac{\rho_1 - \rho_2}{\rho_2} \int_\Omega \phi (\mathbf{v} \cdot \nabla p + \frac{\partial p}{\partial t}) d\mathbf{x}. \tag{2.19}$$

To ensure positivity in the first integral $(2\eta \mathbf{D} + \nu tr(\mathbf{D})\mathbf{I}) : \mathbf{D} \geq 0$, $\eta \geq 0, \nu + \frac{2\eta}{3} \geq 0$. Unfortunately, we have no control over the sign for the second integral. For compressible model 2, the rate of change in the energy for this system of governing equations is given by

$$\frac{d\mathcal{E}}{dt} = -\int_\Omega [\lambda \|\nabla \mu\|^2 + (\tau - \tau_c) : \mathbf{D}] d\mathbf{x} + \frac{\rho_1 - \rho_2}{\rho_2} \int_\Omega \phi (\frac{\partial p}{\partial t} - \frac{d\phi}{dt}) d\mathbf{x}. \tag{2.20}$$

In either models, the energy dissipation can not be rigorously established. On the other hand, for the incompressible model, the energy is defined by

$$E(t) = \int_\Omega [\frac{\rho \|\mathbf{v}\|^2}{2} + F] d\mathbf{x}. \tag{2.21}$$

With the help of the divergence-free condition in the continuity equation, Shen and Yang [32, 33] showed an energy law is available for the incompressible system:

$$\frac{dE}{dt} = -\int_\Omega [\lambda \|\nabla \mu\|^2 + (\tau - \tau_c) : \mathbf{D}] d\mathbf{x} \leq 0. \tag{2.22}$$

One of the traded-offs in enforcing the mass conservation is losing the energy law. Therefore, both compressible models along with the incompressible mixture model in [33] are valid approximately. We note that an analogous phase field equation (to model 1) was also derived using an energy argument in [28].

2.2 Choice of free energy

The free energy F can take different form depending on the applications. In this paper, we consider the free energy density in the following form:

$$F(\phi,\nabla\phi) = k_B T\gamma[\frac{1}{2}\|\nabla\phi\|^2 + f(\phi)], \tag{2.23}$$

where k_B is the Boltzmann constant, T is the absolute temperature, and γ is a parameter with the unit of a number density per unit length. γ is in fact proportional to the product of the number density per unit volume and the square of the persistent length.

We first look at the Ginzburg-Laudau free energy with

$$f(\phi) = \frac{1}{\varepsilon^2}\phi^2(1-\phi)^2 \tag{2.24}$$

for two immiscible fluids, where $\varepsilon > 0$ is a small parameter characterizing the hydrophobic property between the two fluids. Therefore,

$$\frac{\delta F}{\delta\phi} = k_B T\gamma[-\nabla^2\phi + \frac{1}{\varepsilon^2}\phi(1-\phi)(1-2\phi)]. \tag{2.25}$$

We also consider the Flory-Huggins mixing free energy for two immiscible fluids to simulate the phase separation dynamics. The Flory-Huggins mixing free energy density is given by (2.23) with

$$f(\phi) = \frac{1}{\varepsilon^2}[\frac{\phi}{N_1}\ln\phi + \frac{1-\phi}{N_2}\ln(1-\phi) + \chi\phi(1-\phi)], \tag{2.26}$$

where N_1 and N_2 are the polymerization indices for fluid 1 and fluid 2 and χ is the mixing parameter between 0 and 2. If both are viscous fluids, we assume $N_1 = N_2 = 1$. In this case,

$$\frac{\delta F}{\delta\phi} = k_B T\gamma[-\nabla^2\phi + \frac{1}{\varepsilon^2}(\frac{ln\phi}{N_1} + \frac{ln(1-\phi)}{N_2} + \chi(1-2\phi))] + \text{const.} \tag{2.27}$$

2.3 Non-dimensionalization

We denote the characteristic time scale by t_0 and length scale by L_0. The dimensionless variables are defined by

$$\tilde{t} = \frac{t}{t_0}, \tilde{\mathbf{x}} = \frac{\mathbf{x}}{L_0}, \tilde{\mathbf{v}} = \frac{\mathbf{v}t_0}{L_0}, \tilde{p} = \frac{pt_0^2}{\rho_2 L_0^2}. \tag{2.28}$$

We will drop the ˜ on the dimensionless variables in the following. We choose L_0 so that the dimensionless length $L_y = 1$. We use $L_x = 1$ in the following calculations simply for convenience. The dimensionless model parameters are defined by

$$\begin{aligned} &Re_{i,s} = \tfrac{\rho_2 L_0}{t_0\eta_i},\ Re_{i,v} = \tfrac{\rho_2 L_0}{t_0\nu_i},\ (i=1,2)\ \Lambda = \tfrac{\lambda_0 k_B T\gamma}{L_0^4},\ \tilde{\varepsilon} = \tfrac{L_0}{\varepsilon}, \\ &Bi = \phi\tfrac{\rho_1}{\rho_2} + (1-\phi),\ \tfrac{1}{Re_s} = \tfrac{\phi}{Re_{1,s}} + \tfrac{1-\phi}{Re_{2,s}},\ \tfrac{1}{Re_v} = \tfrac{\phi}{Re_{1,v}} + \tfrac{1-\phi}{Re_{2,v}}. \end{aligned} \tag{2.29}$$

Here Re_s and Re_v denotes the Reynolds number corresponding to the shear and volumetric stress, and Λ is the dimensionless mobility parameter. We set $L_y = 1, C = \frac{k_B T\gamma t_0}{L_0^4\rho_2} = 1$ in this study yielding $t_0 = \frac{L_0^4\rho_2}{k_B T\gamma}$.

The dimensionless equations for the two compressible models are given by

$$\begin{cases} \phi_t + \nabla\cdot(\phi\mathbf{v}) = \nabla\cdot(\Lambda\nabla\mu), \\ Bi[\mathbf{v}_t + \mathbf{v}\cdot\nabla\mathbf{v}] = \nabla\cdot(\frac{1}{Re_s}\nabla\mathbf{v}) + \nabla((\frac{1}{Re_s}+\frac{1}{Re_v})\nabla\cdot\mathbf{v}) - \nabla p - \phi\nabla\mu, \\ \nabla\cdot\mathbf{v} = (1-\frac{\rho_1}{\rho_2})[\nabla\cdot(\Lambda\nabla\mu)], \\ \mu = -\Delta\phi + \tilde{f}(\phi) \text{ (Model 1)}, \quad \mu = -\Delta\phi + \tilde{f}(\phi) + (\frac{\rho_1}{\rho_2}-1)p \text{ (Model 2)}, \end{cases} \tag{2.30}$$

where $\tilde{f}(\phi)$ are given by (2.24) or (2.26) with ε replaced by $\tilde{\varepsilon}$.

The above system is subjected to a set of suitable initial and boundary conditions. For example, if the mixture is confined in a domain Ω, the boundary conditions are

$$\frac{\partial\phi}{\partial n}|_{\partial\Omega} = \frac{\partial\mu}{\partial n}|_{\partial\Omega} = 0, \quad \mathbf{v}|_{\partial\Omega} = 0, \tag{2.31}$$

where n is the outward normal.

3 Numerical schemes

Shen and Yang have developed and studied efficient numerical schemes for the incompressible phase field model in great detail in [32, 33]. In this section, we focus on extending their results to the compressible models given for example by (2.15) for the binary fluid mixture. Since the two compressible models do not admit a dissipative energy law, it is not possible to construct energy stable schemes for them. Instead, we shall construct efficient and easy to implement numerical schemes to accommodates the non-vanishing divergence velocity field so as to preserve the mass conservation.

3.1 Discretization in time

To simplify the presentation, we shall present only first-order schemes. In what follows, the superscript n denotes the time level and Δt is the time step size.

Scheme based on a modified projection:

1. Solve (ϕ^{n+1},μ^{n+1}) from:

$$\begin{aligned} &\frac{\phi^{n+1}-\phi^n}{\Delta t} + \nabla\cdot(\phi^n\mathbf{v}^n) = \nabla\cdot(\Lambda\nabla\mu^{n+1}), \quad \frac{\partial\phi^{n+1}}{\partial n}|_{\partial\Omega} = 0, \\ &\mu^{n+1} = -\Delta\phi^{n+1} + \tilde{f}(\phi^n) + \frac{S}{\tilde{\varepsilon}^2}(\phi^{n+1}-\phi^n), \quad \frac{\partial\mu}{\partial n}|_{\partial\Omega} = 0, \end{aligned} \tag{3.1}$$

   where S is a computational parameter and ε is the parameter in the free energy. The last term is added to stabilize the scheme to allow larger step sizes. Its role is to damp the high frequency or short waves in the numerical simulation.

2. Denote

$$\begin{aligned} &Bi^{n+1} = \phi^{n+1}\frac{\rho_1}{\rho_2} + (1-\phi^{n+1}), \quad Re_s^{n+1} = \phi^{n+1}Re_{1,s} + (1-\phi^{n+1})Re_{2,s}, \\ &Re_v^{n+1} = \phi^{n+1}Re_{1,v} + (1-\phi^{n+1})Re_{2,v}; \end{aligned} \tag{3.2}$$

Solve $\tilde{\mathbf{v}}^{n+1}$ from:

$$Bi^{n+1}\left(\frac{\tilde{\mathbf{v}}^{n+1}-\mathbf{v}^n}{\Delta t}+\mathbf{v}^n\cdot\nabla\mathbf{v}^n\right)-\nabla\cdot(Re_s^{n+1}\nabla\tilde{\mathbf{v}}^{n+1})-\nabla((Re_s^{n+1}+Re_\nu^{n+1})\nabla\cdot\mathbf{v}^n)+\nabla p^n=-\phi^{n+1}\nabla\mu^{n+1},$$
$$\tilde{\mathbf{v}}^{n+1}|_{\partial\Omega}=0; \tag{3.3}$$

3. Set $c_0=1$ and solve $p^{n+1}-p^n$ from:

$$-\nabla\cdot\frac{1}{Bi^{n+1}}\nabla(p^{n+1}-p^n)=\frac{1}{\Delta t}\left\{c_0\frac{\rho_2-\rho_1}{\rho_2}[\nabla\cdot(\Lambda\nabla\mu^{n+1})]-\nabla\cdot\tilde{\mathbf{v}}^{n+1}\right\},$$
$$\frac{\partial(p^{n+1}-p^n)}{\partial n}|_{\partial\Omega}=0, \tag{3.4}$$

where Ω is the domain occupies by the fluid mixture.

4. Finally, update

$$\mathbf{v}^{n+1}=\tilde{\mathbf{v}}^{n+1}-\frac{\Delta t}{Bi^{n+1}}\nabla(p^{n+1}-p^n), \tag{3.5}$$

and then goto the next step.

Remarks:

- $S=O(1)$ is a stabilizing computational parameter. We use $S=2$ in all the simulations presented in this paper.
- Setting $c_0=0$ in (3.4), we get the scheme for divergence-free velocity field ($\nabla\cdot\mathbf{v}=0$).
- $\eta=\phi\eta_1+(1-\phi)\eta_2$ and $\nu=\phi\nu_1+(1-\phi)\nu_2$ are the interpolated effective viscosity coefficients.
- A second-order scheme can be constructed as well.

Notice that (3.4)-(3.5) represents a modified pressure-correction projection method. One can easily verify from (3.4)-(3.5) that $\mathbf{v}^{n+1}$ and μ^{n+1} satisfy

$$\nabla\cdot\mathbf{v}^{n+1}=(1-\frac{\rho_1}{\rho_2})[\nabla\cdot(\Lambda\nabla\mu^{n+1})], \tag{3.6}$$

which ensures the mass conservation. However, the step (3.4) in the above involves solving an elliptic equation with $\frac{1}{Bi}$ as the variable coefficient. When $\frac{\rho_2}{\rho_1}$ is large, this step may become very costly. So we propose the following scheme based on the pressure-stabilization technique which only requires solving a pressure Poisson equation. The price we pay for this simplicity is that (3.6) will only be satisfied approximately. This strategy has been proven effective in the numerical solution of the incompressible field phase model [32, 33].

Scheme based on a pressure-stabilization method:

1. Solve (ϕ^{n+1},μ^{n+1}) from:

$$\frac{\phi^{n+1}-\phi^n}{\Delta t}+\nabla\cdot(\phi^n\mathbf{v}^n)=\nabla\cdot(\Lambda\nabla\mu^{n+1}),\quad \frac{\partial\phi^{n+1}}{\partial n}|_{\partial\Omega}=0,$$
$$\mu^{n+1}=-\Delta\phi^{n+1}+\tilde{f}(\phi^n)+\frac{S}{\tilde{\varepsilon}^2}(\phi^{n+1}-\phi^n),\quad \frac{\partial\mu}{\partial n}|_{\partial\Omega}=0. \tag{3.7}$$

2. Denote

$$
\begin{aligned}
&Bi^{n+1} = \phi^{n+1}\frac{\rho_1}{\rho_2} + (1-\phi^{n+1}), \quad Re_s^{n+1} = \phi^{n+1}Re_{1,s} + (1-\phi^{n+1})Re_{2,s},\\
&Re_v^{n+1} = \phi^{n+1}Re_{1,v} + (1-\phi^{n+1})\Re_{2,v};
\end{aligned}
\tag{3.8}
$$

Solve $\tilde{v}^{n+1}$ from:

$$
\begin{aligned}
&Bi^{n+1}\left(\frac{\mathbf{v}^{n+1}-\mathbf{v}^n}{\Delta t} + \mathbf{v}^n\cdot\nabla\mathbf{v}^n\right) - \nabla\cdot(Re_s^{n+1}\nabla\mathbf{v}^{n+1}) - \nabla((Re_s^{n+1}+Re_v^{n+1})\nabla\cdot\mathbf{v}^n) + \nabla p^n = -\phi^{n+1}\nabla\mu^{n+1},\\
&\tilde{\mathbf{v}}^{n+1}|_{\partial\Omega} = 0;
\end{aligned}
\tag{3.9}
$$

3. Set $c_0 = 1$ and solve $p^{n+1} - p^n$:

$$
\begin{aligned}
&-\Delta(p^{n+1}-p^n) = \frac{\rho_{min}}{\Delta t}\left\{c_0\frac{\rho_2-\rho_1}{\rho_2}[\nabla\cdot(\Lambda\nabla\mu^{n+1})] - \nabla\cdot\mathbf{v}^{n+1}\right\},\\
&\frac{\partial(p^{n+1}-p^n)}{\partial n}|_{\partial\Omega} = 0,
\end{aligned}
\tag{3.10}
$$

where $\rho_{min} = \min(\rho_1,\rho_2)$. Go to the next step.

We observe that the step (3.7) is a system of two second-order equations with constant coefficients, the step (3.9) is an elliptic equation with variable coefficients and the step (3.10) is just a Poisson equation. Hence, the above scheme is easy to implement and very efficient.

As in an usual pressure-stabilization method [33] where the divergence-free condition is satisfied approximately, it is clear from (3.10) that $\mathbf{v}^{n+1}$ and μ^{n+1} from the above scheme only satisfy the internal constraint (2.7) approximately with a residue of order $O(\Delta t^2)$. Therefore, the mass is conserved up to a controllable error of order $O(\Delta t^2)$, indepedent of the interfacial width ε.

3.2 Discretization in space

The spatial discretization can be done in either a spectral method or a finite element method or a finite difference method. However, the spatial resolution needs to be fine enough to resolve the interfacial layer. We shall use the high resolution spectral method which requires a significantly less number of unknowns inside the interface as compared with a lower-order method.

We focus in this paper on two-dimensional fluid flows in both drop dynamics as well as mixing dynamics of immiscible binary fluids, and define the computational domain as $\Omega = [0,L_x]\times[0,L_y]$ with the periodic boundary condition in the x-direction. In the y-direction, the boundary conditions are:

$$
\begin{aligned}
&\mathbf{v}(x,y,t) = \mathbf{v}(x+L_x,y,t), \phi(x,y,t) = \phi(x+L_x,y,t),\\
&\mathbf{v}(x,0,t) = \mathbf{v}_0, \mathbf{v}(x,L_y,t) = \mathbf{v}_1, \phi_y(x,0,t) = \phi_y(x,L_y,t) = \phi_{yyy}(x,0,t) = \phi_{yyy}(x,L_y,t) = 0.
\end{aligned}
\tag{3.11}
$$

The boundary conditions of ϕ at $y = 0, L_y$ are interpreted as the flux boundary conditions.

We shall use the Fourier expansion in the x-direction and the Legendre-Galerkin method in the y-direction.

Table 1: Parameter values

Parameter	N	M	g	$Re_{1,s}$	$Re_{2,s}$	ε	$Re_{1,v}$	$Re_{2,v}$	$\frac{\rho_1}{\rho_2}$	Λ
Value	256	256	0	1	1×10^{-2}	0.02	$4.3\times Re_{1,s}$	$4.3\times Re_{2,v}$	$\frac{1}{50}$	1×10^{-6}

4 Numerical results and discussions

We investigate predictive drop dynamics and phase separation dynamics computed using the two distinct classes of models with a focus on the comparison between the phases and the phase boundaries of the mixture. We tabulate the dimensionless parameters used in the simulations in Table 1, where N and M denote the number of grid points in x and y direction, respectively. These are chosen based on our previous experience with the two-phase fluid [32, 33].

We first consider the drop dynamics of fluid 1 immersed in fluid 2 and denote the volume fraction of fluid 1 as ϕ. For presentation purposes, we relabel the models as follows in the figures: Model 1: incompressible model, Model 2: compressible model 1, Model 3: compressible model 2.

4.1 Drop dynamics

We first simulate a lighter fluid (fluid 1, $\phi = 1$) drop immersed in a heavier fluid (fluid 2, $\phi = 0$). The density ratio we choose for this numerical example is $\rho_1 : \rho_2 = 1 : 50$ and viscosity ratio $1 : 100$. In this setting, the lighter drop will rise in the fluid channel (computational domain). The simulated results using the compressible models and the incompressible model for mixtures agree with each other qualitatively. The velocity components, pressure and the drop profiles obtained using the three phase field models are shown in Figures 1-3, respectively. In the simulations, the lighter fluid drop rises; the rising drop pushes the fluid in the front aside and pushes the fluid downward on the side of the fluid domain. The horizontal and the vertical velocity component are plotted in Figures 1 and 2, respectively. The pressure around the drop remains low, which is shown in Figure 3. The drop shapes obtained using the three distinct models are contrasted at a selected time $t = 3.6$ in Figure 4 along with the deviations between the velocity components of each pair of models. The predictions from model 1 and 2 are close relative to that from model 3. The deviations in general fall into the range of $O(10^{-2})$. The velocity field superimposed by the drop profile is shown in Figure 5, where a pair of vortices are shown explicitly.

We then repeat the simulation with a heavier fluid drop sediments in a lighter fluid. The density ratio is reversed to $\rho_1 : \rho_2 = 50 : 1$ and the viscosity ratio is reversed to $100 : 1$. The behavior described above for the rising drop reverses. This time, the predictions between model 1 and model 2 and those between model 2 and model 3 are qualitatively the same; model 3 predicts the fastest drop sedimentation among all three. To save space, we suppress the demonstration of the numerical results pertinent to this simulation.

In summary, the model predictions in both drop rising and drop sedimentation agree qualitatively. In these cases, the interfacial layer between the two immiscible fluids are thin and the volume fraction of the fluid involved in the mixing/interfacial zone is small. Consequently, the deviation among the model predictions are small. We anticipate this scenario will change as the mixing/interfacial layer gets larger and the volume fraction of the fluid involved in mixing becomes significant. We next examine an example of fluid mixing/demixing where the mixing zone is significantly larger.

4.2 Phase separation dynamics of immiscible binary fluids

Figures 6-9 depict the phase portrait of the mixture during phase separation and the corresponding velocity components as well as the pressure field at selected time. In Figure 6, the value of the volume

fraction ϕ is plotted as a color map. The compressible models (model 2 and model 3) give well separated islands while the incompressible model (model 1) predicts only slightly modified phase landscape. Figures 7 and 8 supports this with a much elevated velocity field in the compressible models than in the incompressible model. Moreover, the flow pattern is drastically different between the predictions obtained from different classes of models. Figure 9 portraits the pressure field, which correlates well with the phase portrait of the mixture given by the level sets of the volume fraction ϕ. The difference between the two classes of models are *significant* in this numerical example. The drastic difference between the model predictions is an amplification of the difference in the fundamental physical mechanism on mass conservation in a much larger mixing zone in contrast to the previous drop dynamics.

If these examples show the behavior of the transient solution, the next set of figures (Figures 10-13) portrait the solutions up to nearly quasi-static states. The phase behavior predicted by the incompressible model (Model 1) is distinct quantitatively from those by the compressible models (Figure 10). The prediction on the velocity field and the pressure field made by the incompressible model and by the compressible ones are completely different. Whereas, the difference between the compressible model predictions is minimal.

If we were to impose the constraint on the conservation of the total volume of each separate phase, the predictions from the compressible models should be more credible since they also conserves the mass, which is fundamentally important.

5 Conclusion

A pair of phase field models that conserve mass, momentum and total volume for each individual phase of immiscible binary fluid mixtures are formulated. The mass-average velocity becomes non-solenoidal when the density ratio between the two fluids is not unity. Consequentially, the new phase field theories are compressible although a global volume conservation for each phase can be maintained over the entire material volume. The commonly used phase field model for binary fluid mixtures is the model we refer to as the incompressible model in this paper, in which the continuity equation is approximated by a divergence free condition; the resulting theory preserves the material volume but not the mass.

The deviation between the predictions by the compressible models and the incompressible one depend on the size of the mixing zone. When the size of the mixing zone is small compared to the entire fluid domain, the model predictions agree qualitatively. However, when the mixing zone is large, the two classes of models describe two quite different dynamics (in both transient and quasi-steady state). One numerical example on a drop dynamics of one fluid drop immersed in another immiscible fluid matrix and the other on the phase separation of immiscible binary fluid mixtures are carried out to illustrate the point. From the hydrodynamics point of view, it is apparent that the fundamental conservation laws of fluids must be obeyed. Therefore, the mass conservation should be respected in any faithful simulations employing the phase field formulation when the mixing zone is large. The predictions made by the compressible models are consistent in the two numerical examples, and therefore are credible regardless of the size of mixing zone.

Acknowledgment

The work of Jie Shen is partially supported by NSF grants DMS-0915066 and AFOSR FA9550-08-1-0416; Qi Wang's research is partially supported by NSF grants DMS-0819051, DMS-0908330, SC EPSCOR award and the USC startup fund; X. Yang's research is partially supported by the ARO grant W911NF-09-1-0389 and the USC startup fund.

References

[1] Bird, Stewart, and Lightfoot, **Transport Phenomena**, John Wiley and Sons, 2002.

[2] Probstein, **Physicochemical Hydrodynamics,** John Wiley and Sons, 1994.

[3] B. Bird, R. Armstrong, O. Hassager, **Dynamics of Polymeric Liquids**, 2nd Ed., Vol. 2, John Wiley and Sons, New York, 1987.

[4] A. N. Beris and B. Edwards, **Thermodynamics of Flowing Systems**, Oxford University Press, Oxford, 1994.

[5] B. Lindley, Q. Wang and T. Zhang, Multicomponent models for biofilm flows, Discrete and Continuous Dynamic Systems- Series B,15(2) (2011), 417-456.

[6] J. W. Cahn and J. E. Hilliard. Free energy of a nonuniform system. i: interfacial free energy. J. Chem. Phys., 28 (1959), 258–267.

[7] J. W. Cahn and J. E. Hilliard. Free energy of a nonuniform system-iii: Nucleation in a 2-component incompressible fluid. J. Chem. Phys., 31(3) (1959), 688–699.

[8] L. Q. Chen and W. Yang, Computer simulation of the dynamics of a quenched system with large number of non-conserved order parameters, Phys. Rev. B, 50 (1994), 15752-15756.

[9] L. Q. Chen, Phase-field modeling for microstructure evolution, Annu. Rev. Mater. Res., 32 (2002), 113-140.

[10] L. Q. Chen and Y. Wang, The Continuum Field Approach to Modeling Microstructural Evolution, J. Miner Met. Mater. Soc. 48 (12) (1996), 13-18.

[11] M. Doi, **Introduction to Polymer Physics,** Clarendon Press, Oxford, 1996.

[12] Q. Du, C. Liu, R. Ryham and X. Wang, Phase field modeling of the spontaneous curvature effect in cell membranes, Comm. Pur. Applied. Anal., 4 (2005), 537-548.

[13] Q. Du, C. Liu, R. Ryham and X. Wang, A phase field formulation of the Willmore problem, Nonlinearity, 18 (2005), 1249-1267.

[14] Q. Du, C. Liu and X. Wang, A Phase Field Approach in the Numerical Study of the Elastic Bending Energy for Vesicle Membranes, J. Comp. Phy., 198 (2004), 450-468.

[15] Q. Du, C. Liu and X. Wang, Retrieving topological information for phase field models, SIAM Journal on Applied Mathematics, 65 (2005), 1913-1932.

[16] Q. Du, C. Liu and X. Wang, Simulating the Deformation of Vesicle Membranes under Elastic Bending Energy in Three Dimensions, J. Comp. Phys., 212 (2005), 757-777.

[17] M. G. Forest and Q. Wang, Hydrodynamic theories for blends of flexible polymer and nematic polymers, Physical Review E, 72 (2005), 041805.

[18] M. G. Forest, Q. Liao and Qi Wang, 2-D Kinetic Theory for Polymer Particulate Nanocomposites, Communication in Computational Physics, 7 (2) (2010), 250-282.

[19] J. J. Feng, C. Liu, J. Shen and P. Yue, Transient Drop Deformation upon Startup of Shear in Viscoelastic Fluids, Fluids. Phys. Fluids, 17 (2005), 123101.

[20] P. J. Flory, **Principles of Polymer Chemistry**, Cornell University Press, Ithaca, NY, 1953.

[21] R. Hobayashi, Modeling and numerical simulations of dendritic crystal growth, Physica D, 63 (1993), 410-423.

[22] A. Karma and W. Rappel, Phase-Field Model of Dendritic Sidebranching with Thermal Noise, Phys. Rev. E, 60 (1999), 3614-3625.

[23] 1.Jinsong Hua, Ping Lin, Chun, Liu, Qi Wang, Energy Law Preserving C^0 Finite Element Schemes for Phase Field Models in Two-phase Flow Computations, J. Comp. Phys., 230 (19) (2011), 7115-7131.

[24] C. Liu and N. J. Walkington, An Eulerian description of fluids containing visco-hyperelastic particles, Arch. Rat. Mech. Ana., 159 (2001), 229-252.

[25] C. Liu and J. Shen, A phase field model for the mixture of two incompressible fluids and its approximation by a fourier-spectral method, Physica D, 179 (2003), 211-228.

[26] Y. Li, S. Hu, Z. Liu, and L. Chen, Phase-field model of domain structures in ferroelectric thin films, Appl. Phys. Lett., 78 (2001), 3878-3880.

[27] W. Lu and Z. Suo, Dynamics of nanoscale pattern formation of an epitaxial monolayer, J. Mech. Phys. Solids, 49 (2001), 1937-1950.

[28] J. Lowengrub and L.Truskinovsky, Quasi-incompressible Cahn-Hilliard fluids and topological transitions, R. Soc. Lond. Proc. Ser. A Math. Phys. Eng. Sci., 454 (1998), 2617–2654.

[29] G. McFadden, A. Wheeler, R. Braun, S. Coriell, and R. Sekerka, Phys. Rev. E, 48 (1998), 2016-2024.

[30] D. J. Seol, S. Y. Hu, Y. L. Li, J. Shen, K. H. Oh and L. Q. Chen, Three-dimensional Phase-Field Modeling of Spinodal Decomposition in Constrained Films, Acta Materialia 51 (2003), 5173-5185.

[31] J. Shen and X. Yang, An efficient moving mesh spectral method for the phase-field model of two phase flows, J. Comput. Phys., 228 (2009), 2978-2992.

[32] J. Shen and X. Yang, Energy Stable Schemes for Cahn-Hilliard phase-field model of two-phase incompressible flows, Chinese Ann. Math. series B, 31 (2010), 743-758.

[33] J. Shen and X. Yang, A phase-field model and its numerical approximation for two-phase incompressible flows with different densities and viscositites, SIAM J. Sci. Comput., 32(3) (2010), 1159-1179.

[34] E. Tadmor, R. Phillips, and M. Ortiz, Mixed Atomistic and Continuum Models of Deformation in Solids, Langmuir, 12 (1996), 4529-4534.

[35] X. Wang, Asymptotic Analysis of Phase Field Formulations of Bending Elasticity Models, submitted to SIAM Mathematical Analysis (2006).

[36] Q. Wang, W. E, C. Liu, and P. Zhang, Kinetic theories for flows of nonhomogeneous rodlike liquid crystalline polymers with a nonlocal intermolecular potential, Physical Review E, 65(5) (2002), 0515041-0515047.

[37] Q. Wang, A hydrodynamic theory of nematic liquid crystalline polymers of different configurations, Journal of Chemical Physics, 116 (2002), 9120-9136.

[38] Q. Wang, M. G. Forest and R. Zhou, A hydrodynamic theory for solutions of nonhomogeneous nematic liquid crystalline polymers with density variations, J. of Fluid Engineering, 126 (2004), 180-188.

[39] Y. Wang and C. L. Chen, Simulation of microstructure evolution. In Methods in Materials Research, Ed. E. N. Ksufmann, R. Abbaschian, A. Bocarsly, C. L. Chien, D. Dollimore, et al., (1999), 2a3.1-2a3.23.

[40] A. Wheeler, G. McFadden, and W. Boettinger, Proc. R. Soc. London Ser. A, 452 (1996), 495-525.

[41] S. M. Wise, J. S. Lowengrub, J. S. Kim and W. C. Johnson, Efficient phase-field simulation of quantum dot formation in a strained heteroepitaxial film, Superlattices and Microstructures, 36 (2004) 293-304.

[42] X. Yang, J. Feng, C. Liu and J. Shen, Numerical simulations of jet pinching-off and drop formation using an energetic variational phase-field method, J. Comput. Phys., 218 (2006), 417-428.

[43] P. Yue, J. J. Feng, C. Liu, and J. Shen, A diffuse-interface method for simulating two-phase flows of complex fluids, J. Fluid Mech., 515 (2004), 293–317.

[44] P. Yue, J. J. Feng, C. Liu, and J. Shen, Diffuse-interface simulations of drop coalescence and retraction in viscoelastic fluids, J. Non-Newtonian Fluid Mech., 129 (2005), 163-176.

[45] T. Y. Zhang, N. Cogan, and Q. Wang, Phase Field Models for Biofilms. II. 2-D Numerical Simulations of Biofilm-Flow Interaction, Communications in Computational Physics, 4 (2008), 72-101.

[46] T. Y. Zhang and Q. Wang, Cahn-Hilliard vs Singular Cahn-Hilliard Equations in Phase Field Modeling, Communication In CP, 7(2) (2010), 362-382.

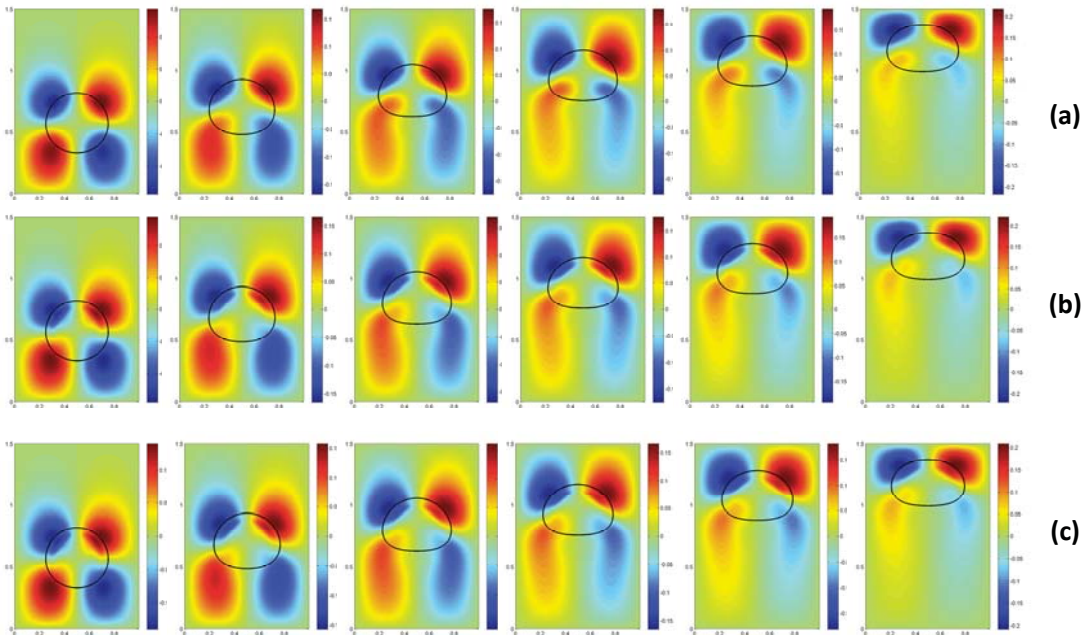

Figure 1: The horizontal velocity component in the case of a lighter drop immersed in a heavier fluid with density ratio $\rho_1 : \rho_2 = 1 : 50$ at time $t = 0.6, 1.2, 1.8, 2.4, 3, 3.6$. (a) M1 (Model 1); (b). M2 (Model 2); (c). M3 (Model 3). Each figure is superimposed by the shape of the drop, i.e. the zero contour curve of the phase-field function ϕ, at the corresponding time.

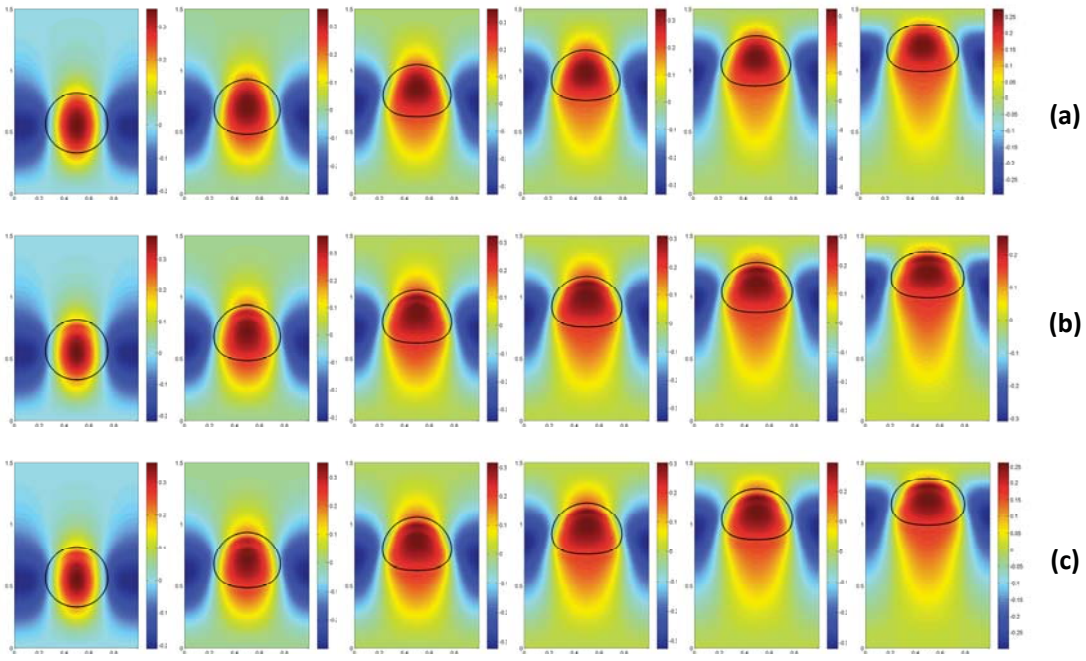

Figure 2: The vertical velocity component in the case of a lighter drop immersed in a heavier fluid with density ratio $\rho_1 : \rho_2 = 1 : 50$ at $t = 0.6, 1.2, 1.8, 2.4, 3, 3.6$. (a) M1, (b). M2, (c). M3. Each figure is superimposed by the shape of the drop, i.e. the zero contour curve of the phase-field function ϕ, at the corresponding time.

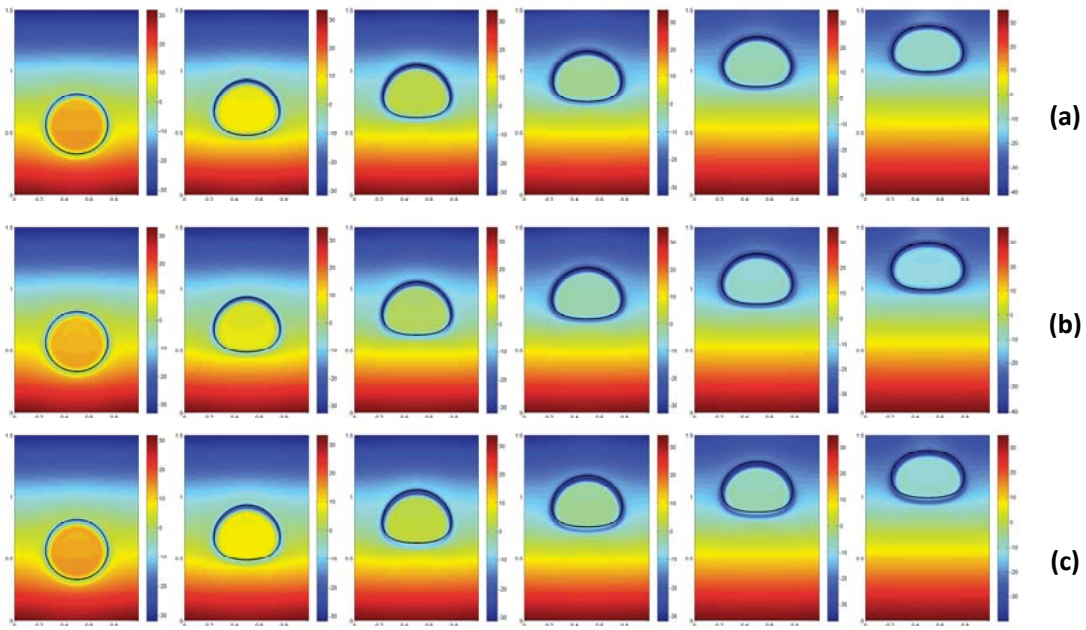

Figure 3: The pressure field in the case of a lighter drop immersed in a heavier fluid with density ratio $\rho_1 : \rho_2 = 1 : 50$ at $t = 0.6, 1.2, 1.8, 2.4, 3, 3.6$. (a) M1, (b). M2, (c). M3. Each figure is superimposed by the shape of the drop, i.e. the zero contour curve of the phase-field function ϕ, at the corresponding time.

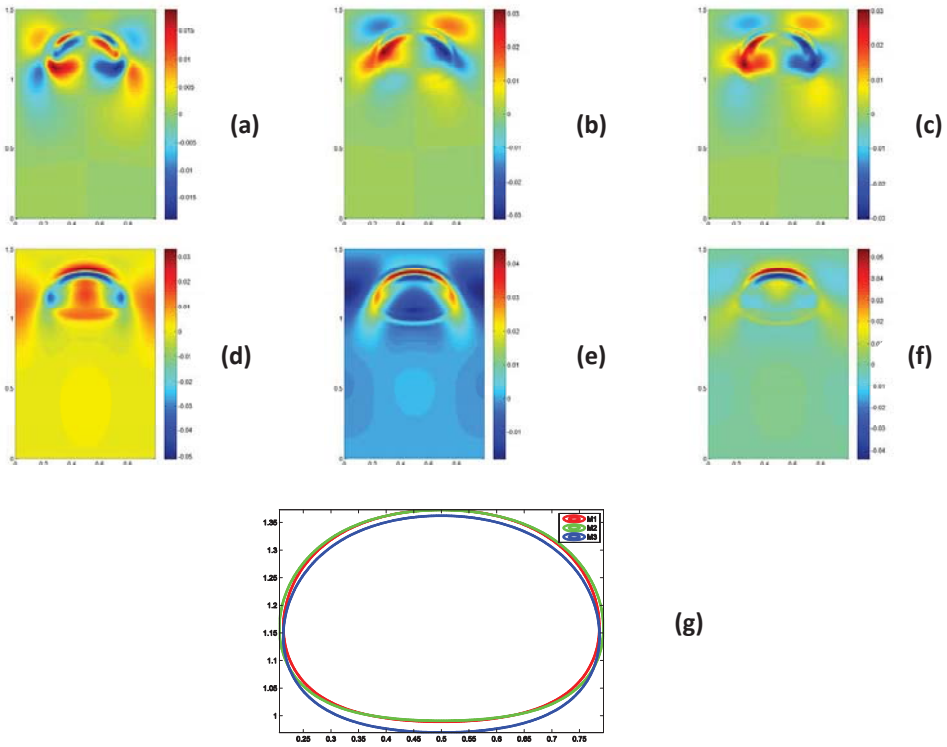

Figure 4: The velocity difference between pairs of the phase field models investigated. (a) $u(M1) - u(M2)$, (b) $u(M1) - u(M3)$, (c) $u(M2) - u(M3)$, (d) $v(M1) - v(M2)$, (e) $v(M1) - v(M3)$, (f) $v(M2) - v(M3)$, (g) Comparisons of the zero contour curves of ϕ for all three models. The results are based on the solutions at $t = 3.6$.

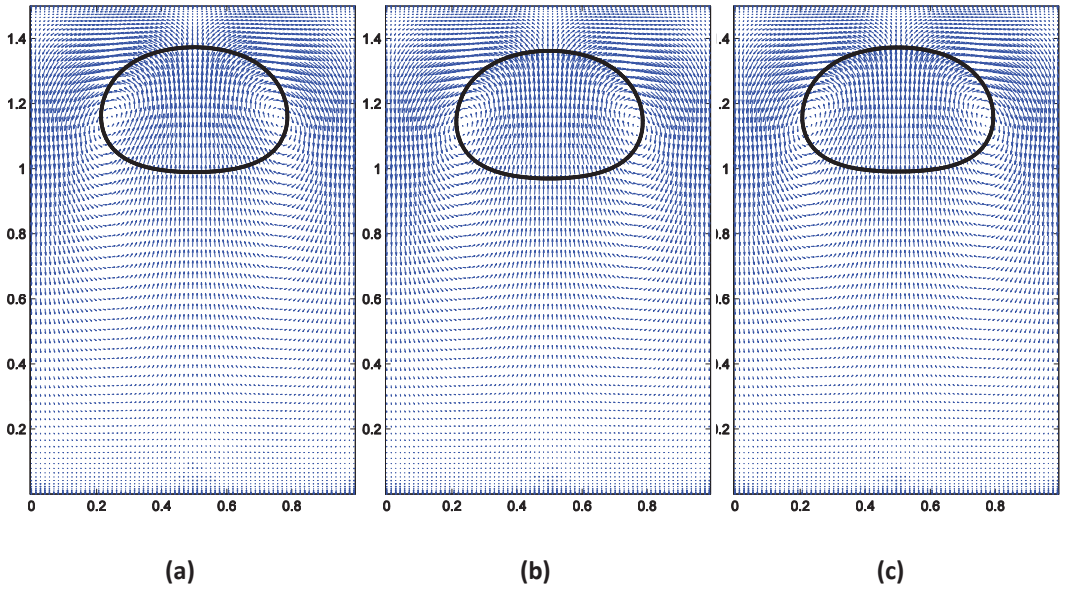

Figure 5: The velocity field superimposed by the shape of the drop at $t = 3.6$ for the three models. (a) $M1$ (b) $M2$, (c) $M3$.

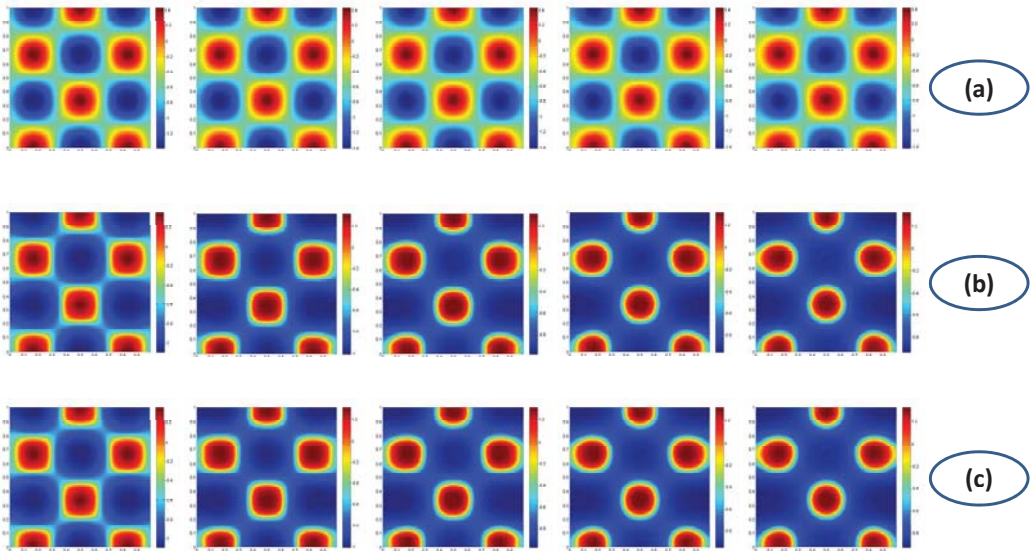

Figure 6: The phase portrait of the binary fluid mixing with the Flory-Huggins energy for all three models at $t = 0.1, 0.2, 0.3, 0.4, 0.5$. (a) $M1$, (b) $M2$, (c) $M3$.

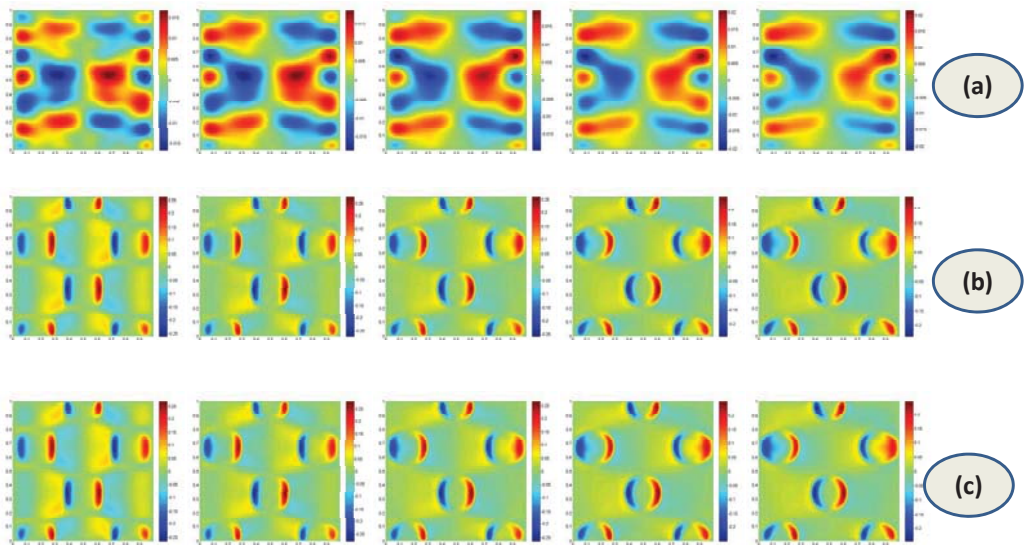

Figure 7: The velocity component u at $t = 0.1, 0.2, 0.3, 0.4, 0.5$ in the case of binary fluid mixing for all three models. (a) $M1$, (b) $M2$, (c) $M3$.

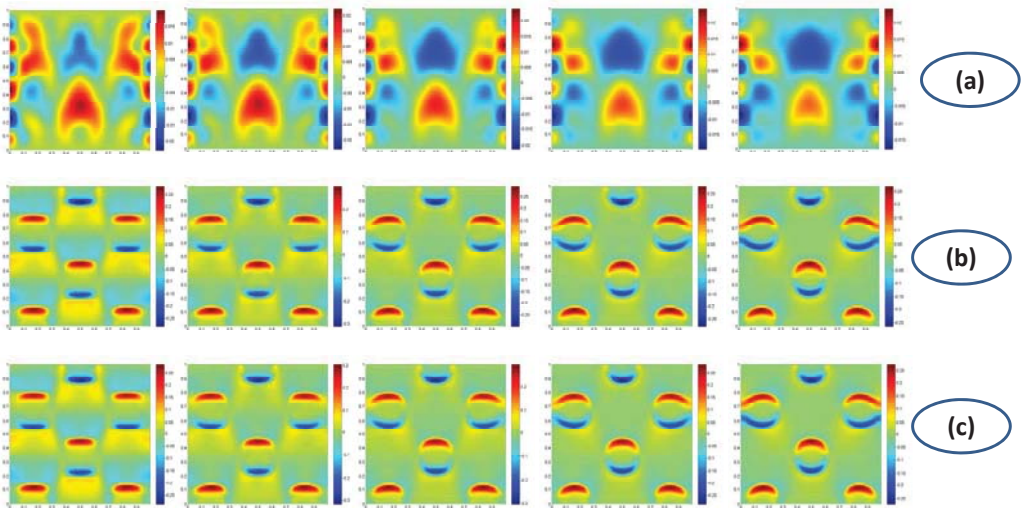

Figure 8: The velocity component v at $t = 0.1, 0.2, 0.3, 0.4, 0.5$ in the case of binary fluid mixing for all three models. (a) $M1$, (b) $M2$, (c) $M3$.

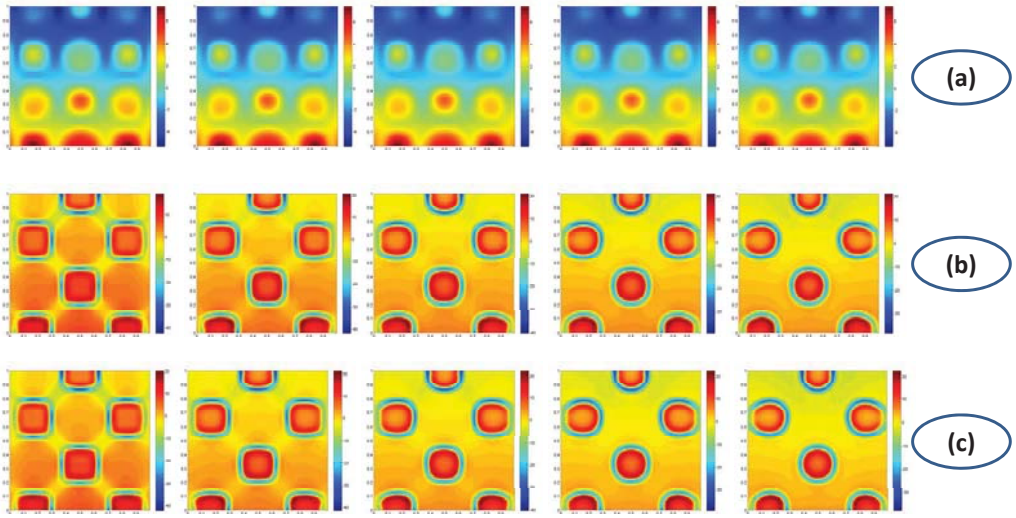

Figure 9: The hydrodynamic pressure p at $t = 0.1, 0.2, 0.3, 0.4, 0.5$ in the case of binary fluid mixing for all three models. (a) $M1$, (b) $M2$, (c) $M3$.

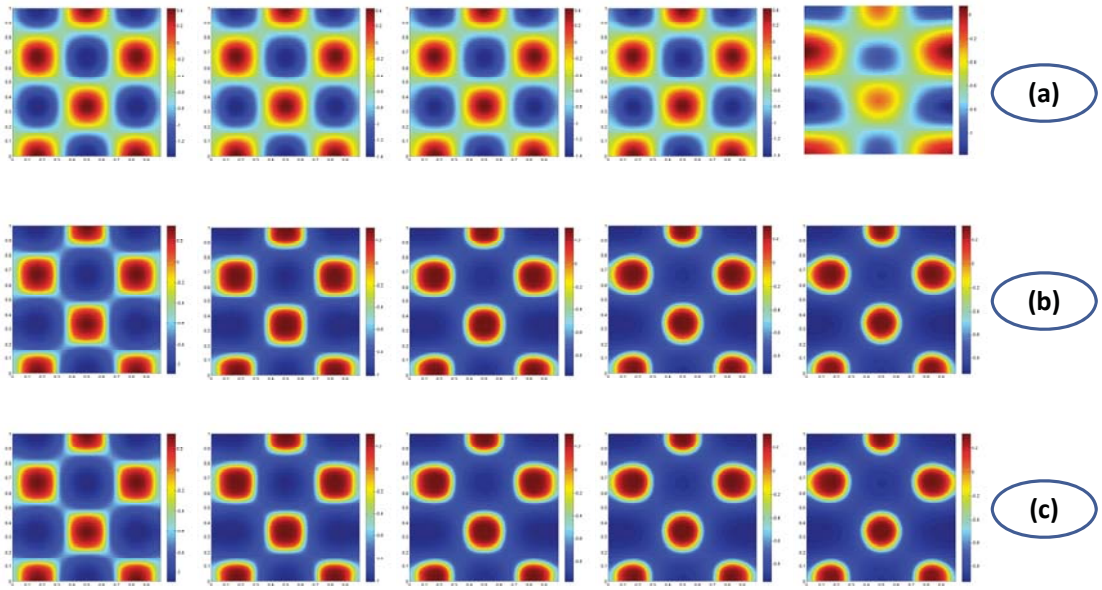

Figure 10: The phase portrait of the binary fluid mixing with the Flory-Huggins energy for all three models at $t = 0.1, 0.2, 0.3, 0.4, 15$. (a) $M1$, (b) $M2$, (c) $M3$.

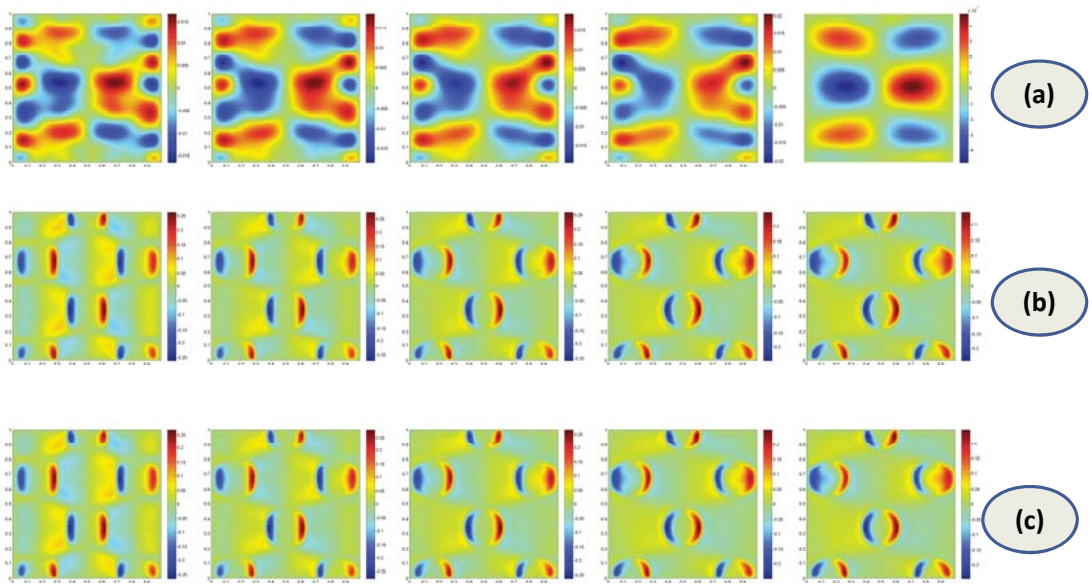

Figure 11: The velocity component u at $t = 0.1, 0.2, 0.3, 0.4, 15$ in the case of binary fluid mixing for all three models. (a) $M1$, (b) $M2$, (c) $M3$. The solutions nearly reach quasi-steady state at $t = 15$.

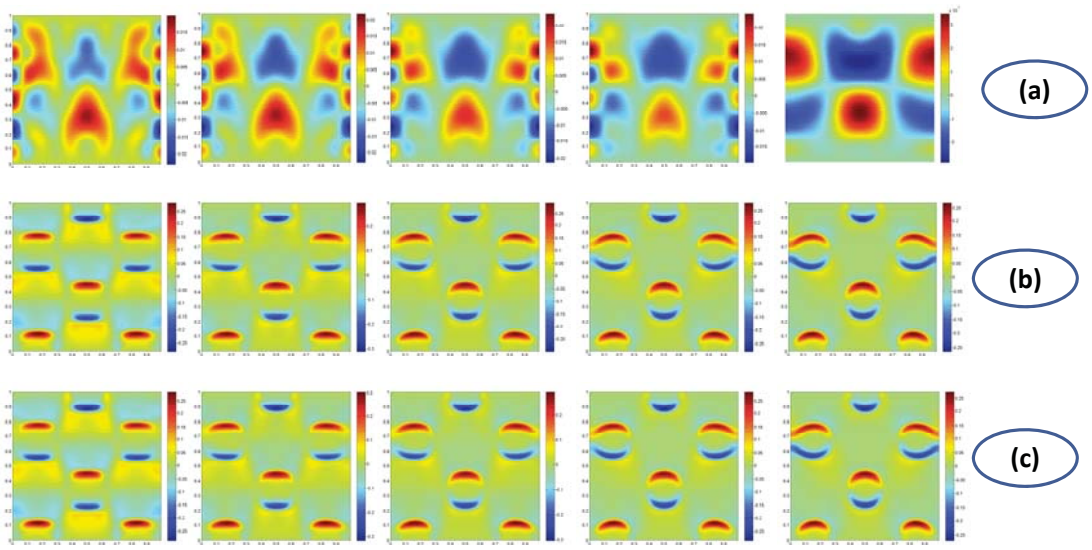

Figure 12: The velocity component v at $t = 0.1, 0.2, 0.3, 0.4, 15$ in the case of binary fluid mixing for all three models. (a) $M1$, (b) $M2$, (c) $M3$. The solutions nearly reach quasi-steady state at $t = 15$.

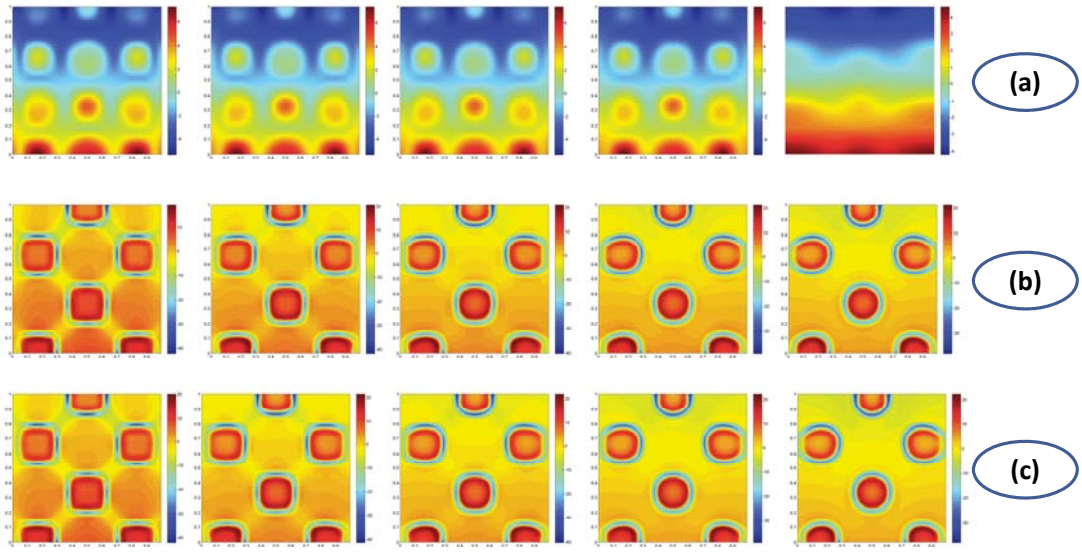

Figure 13: The hydrodynamic pressure p at $t = 0.1, 0.2, 0.3, 0.4, 15$ in the case of binary fluid mixing for all three models. (a) $M1$, (b) $M2$, (c) $M3$. The solutions nearly reach quasi-steady state at $t = 15$.